Magnetic Properties of Terminal Iodinated Nitroxide Radical Liquid Crystals

Takuya Akita,[1] Taira Yamazaki,[1] Yoshiaki Uchida*[1,2] and Norikazu Nishiyama[1]

[1]Graduate School of Engineering Science, Osaka University, 1-3 Machikaneyama-cho, Toyonaka, Osaka 560-8531.

[2]PRESTO, Japan Science and Technology Agency (JST), 4-1-8 Honcho, Kawaguchi, Saitama 332-0012.

* E-mail: yuchida@cheng.es.osaka-u.ac.jp

Abstract

We designed and synthesized terminal iodinated nitroxide radical liquid crystalline compounds (NR-LCs) with octyloxy side chain (±)-**8-I** and dodecyloxy side chain (±)-**12-I** to understand the substitution effects of an iodine atom on the phase transition behavior and on the magnetic properties in crystalline (Cr), liquid crystalline (LC) and isotopic (Iso) phases. These NR-LCs show monotropic nematic phases because the iodine atom is too short and apolar as a terminal group to stabilize LC phases. Furthermore, the SQUID magnetometry and electron paramagnetic resonance (EPR) spectroscopy indicate that the magnetic properties in Cr phase depend on the length of the alkoxy side chain; antiferromagnetic interactions occur in (±)-**8-I**, whereas ferromagnetic interactions occur in (±)-**12-I**, and the paramagnetic susceptibility of (±)-**8-I** slightly decreases ($\bar{J} < 0$) and that of (±)-**12-I** abruptly increases ($\bar{J} > 0$) at each of the Cr-to-Iso phase transitions. These results suggest that the most frequent type of the magnetic interactions in LC and Iso phases is similar to those in the Cr phases among the various types of intermolecular magnetic interactions induced by the inhomogeneous intermolecular contacts.

Keywords

Nitroxide radical; Paramagnetic liquid crystal; Magnetic property; Electron paramagnetic resonance spectroscopy

1. Introduction

Recently, all-organic paramagnetic rod-like liquid crystalline compounds containing a five-membered ring nitroxide radical (NR) moiety in the molecular core (NR-LCs) have attracted a great deal of attention because of their fascinating properties in externally applied fields. For example, some of them show liquid crystalline (LC) phases such as nematic (N), chiral N (N*), smectic A (SmA), chiral SmA (SmA*), smectic C (SmC) and chiral SmC (SmC*) phases [1–3], and their molecular reorientation occurs in uniform magnetic and electric fields [4–6]. Furthermore, their magnetic properties can be changed by the electric-field-induced molecular reorientation in their

SmC* phase [5]. In addition, NR droplets are attracted by a magnet [7], and spin glass-like inhomogeneous ferromagnetic interactions (Magneto-LC effects) occur in the LC phases of rod-like NR compounds [8]; the magneto-LC effects lead to an abrupt increase of paramagnetic susceptibility at crystalline (Cr)-to-LC or Cr-to-isotropic (Iso) phase transitions (positive magneto-LC effects, $\bar{J} > 0$). In contrast, some of the rod-like NR compounds show averagely weak antiferromagnetic interactions (negative magneto-LC effects, $\bar{J} < 0$) [3].

One of the factors to decide the sign and magnitude of the magneto-LC effects is the direction and distance between each pair of molecules contacting with each other in LC or Iso phases [8]. The manner of the intermolecular contacts depends both on phases and on molecular structures. In fact, the modification of a mesogen core and side chains, which are typical components of calamitic LC compounds, is effective to tune the phase transition behavior; e.g., longer side chains induce a highly-ordered smectic (Sm) phases than N or N* phases [3]. Moreover, in some cases, a hydrogen-bonded mesogen core can stabilize the LC phases of NR-LCs [9] because the hydrogen-bonded core plays the same role as the covalent-bonded one [10]. Furthermore, since the introduction of the hydrogen-bonding generally decreases the orientational order parameter of the LC phases [11,12], the inhomogeneity increases and magneto-LC effects become twice as strong as those of the corresponding covalent-bonded analogue [9]. Furthermore, the molecular chirality also considerably influences the sign and magnitude of the magneto-LC effects; even if the racemic sample of a chiral NR compound shows the negative effects, the enantiomerically enriched sample of the same compound shows the positive effects [3]. To enhance the magneto-LC effects by the precise design of molecular structures, more detailed understanding of the origin of the magneto-LC effects is needed.

In this paper, we focus on the correlation between the magnetic interactions in Cr phases and those in LC or Iso phases. In a Cr phase of an ordinary organic monoradical, there are only one or two types of intermolecular magnetic interactions. In contrast, in a fluid phase of the same compound, there should be countless types of the magnetic interactions. However, there could be only intermolecular magnetic interactions similar to those of the Cr phases in some fluid phases. To obtain such compounds, we have designed and synthesized compounds (±)-**8-I** and (±)-**12-I** with a terminal iodine atom, whose bulkiness and ability to form the halogen-bonding could induce the similarity of the molecular packing manners in LC and Cr phases. Here, we report the synthesis of (±)-**8-I** and (±)-**12-I** and discuss the phase transition behaviors and the magneto-LC effects in the LC phases by means of SQUID magnetometry and electron paramagnetic resonance (EPR) spectroscopy, which has proved to be an excellent tool to analyze the magnetic interactions operating in the LC and Iso phases of rod-like NR compounds around ambient temperature [8].

2. Material and methods

Mass spectra were recorded on a JEOL JMS-700. IR spectra were recorded with a SHIMADZU IRAffinity-1. Elemental analyses (CHN) were obtained on a PerkinElmer 2400II. EPR spectra were recorded with a JEOL JES-FE1XG. Magnetization was recorded with a QUANTUN DESIGN MPMS-3. Phase transition behaviors were determined by differential scanning calorimetry (DSC) (SHIMADZU DSC-60), polarized optical microscopy (Olympus BX51) and X-ray diffraction (XRD) measurement. A hot stage (Japan High Tech, 10083) was used as the temperature control unit for the microscopy. For variable temperature XRD measurement, the data collections were performed on a Rigaku RINT2200/PC-LH diffractometer using Cu-Kα radiation with 1.5418 Å. Unless otherwise noted, solvents and reagents were reagent grade and used without further purification. X-ray crystal structures were analyzed using a Rigaku Osmic VariMax diffractometer with graphite-monochromated Mo Kα radiation (λ = 0.71075 Å). Tetrahydrofuran (THF) that was used for electron paramagnetic resonance (EPR) spectroscopy was distilled from sodium/benzophenone ketyl under nitrogen.

*2.1. Synthesis of (±)-**8-I** and (±)-**12-I***

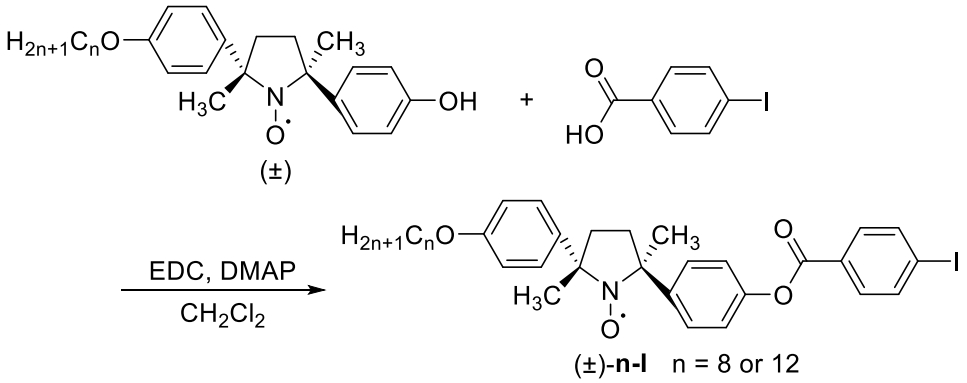

Scheme 1 Synthesis and molecular structures of (±)-**8-I** and (±)-**12-I**.

Racemates of phenolic NR compounds were prepared as a precursor according to the previously reported procedure [13]. The phenolic NR compounds were esterified with 4-iodobenzoic acid to afford (±)-**8-I** and (±)-**12-I** as shown in **Scheme 1**. Dichloromethane (50 mL) was charged with the phenolic NR compound (0.30 mmol), the 4-iodobenzoic acid (0.33 mmol), 1-(3-dimethylaminopropyl)-3-ethylcarbodiimide hydrochloride (EDC·HCl, 0.45 mmol), and 4-(dimethylamino)pyridine (DMAP, 0.09 mmol). After the mixture was stirred for 12 h at room temperature, reaction solution was added saturated aqueous $NaHCO_3$ (50 mL), and extracted with diethyl ether (50 mL × 2). The extract was dried over $MgSO_4$ and evaporated. The residue was purified by column chromatography on silica gel (hexane/ethyl acetate = 9/1) and recrystallized from hexane to afford the ester (±)-**8-I** and (±)-**12-I** as yellow crystals (yield 60–70%).

(±)-**8-I**: IR ν (KBr): 2936, 2853, 1736, 1508, 1261, 1202, 1171, 1005, 748, 600 cm^{-1}; HRMS: Calcd. for $C_{33}H_{39}INO_4$ $[M]^+$: 640.1924, Found 640.1922; Anal. Calcd. for $C_{33}H_{39}INO_4$: C, 61.88; H, 6.14; N, 2.19; Found: C, 61.88; H, 6.24; N, 2.14.

(±)-**12-I**: IR ν (KBr): 2920, 2851, 1734, 1508, 1248, 1175, 1076, 1007, 743, 586 cm^{-1}; HRMS: Calcd. for $C_{37}H_{47}INO_4$ $[M]^+$: 696.2550, Found 696.2549; Anal. Calcd. for $C_{37}H_{47}INO_4$: C, 63.79; H, 6.80; N, 2.01; Found: C, 64.04; H, 6.65; N, 1.98.

2.2. Determination of phase transition behaviors

The phase transition behaviors of (±)-**8-I** and (±)-**12-I** are characterized by DSC analyses, polarized optical microscopy and variable temperature XRD analyses. For DSC analyses, each powder sample of 2–3 mg was put into an aluminum sample pan. Each sample was heated to 130 °C and cooled to room temperature at a rate of 5 °C/min under a flow of N_2 gas. For polarized optical microscopy, each sample was introduced by capillary action into an about 10-μm thick handmade glass sandwich cell in which the inner surfaces of the two glass substrates were untreated. For XRD analyses, line profiles were recorded in the first heating and cooling processes.

2.3. Evaluation of magnetic properties

The temperature dependence of molar magnetic susceptibility measured on a SQUID magnetometer at a field of 0.5 T in the temperature range of 2–300 K in the first heating process. Each sample was enclosed in a DSC aluminum pan to prevent the sign inversion of the total magnetic susceptibility of samples in high temperature ranges.

The X-band EPR spectra were measured under an applied magnetic field of 0.33 T. Their g values and hyperfine coupling constants (a_N) were determined by the measurements of THF solutions at room temperature. For the evaluation of paramagnetic susceptibility, four measurements of each powder and melt samples were performed at each temperature. Each sample was sealed in a quartz tube. Sweep time was 90 s, modulation width was 0.2 mT and time constant was 0.03 s.

*2.4 Determination of the crystal structure of (±)-**8-I***

Crystals of (±)-**8-I** suitable for XRD studies were prepared by recrystallization from hexane, and analyzed using an X-ray diffractometer. The X-ray crystal structure of (±)-**8-I** was solved by direct methods and refined using the full-matrix least-squares method. In subsequent refinements, the function $\sum\omega(F_o^2-F_c^2)^2$ was minimized, where F_o and F_c are the observed and calculated structure factor amplitudes, respectively. The positions of non-hydrogen atoms were determined from difference Fourier electron-density maps and refined anisotropically. All calculations were performed with the Crystal Structure crystallographic software package.

3. Results and Discussion

3.1. Phase transition behavior

The phase transition behaviors of (±)-**8-I** and (±)-**12-I** are characterized by DSC analyses at a scanning rate of 5 °C/min upon heating and cooling processes as shown in **Figure 1** and by polarized optical microscopy as shown in **Figure 2**. In the heating processes, (±)-**8-I** shows a Cr-to-Iso phase transition at 95.6 °C, whereas (±)-**12-I** shows Cr-to-Cr phase transitions at 78.1, 83.1 and 95.5 °C and a Cr-to-Iso phase transition at 101.9 °C. During the cooling process, both (±)-**8-I** and (±)-**12-I** exhibit similar phase transition behaviors. Both (±)-**8-I** and (±)-**12-I** exhibit Iso-to-LC phase transitions at 74.1 °C and 67.8 °C, respectively; Schlieren textures typical of N phases were observed at 55 °C in both cases as shown in **Figure 2** [14]. These supercooled LC phases remain stable above around room temperature. Furthermore, variable temperature X-ray diffraction analyses of (±)-**8-I** and (±)-**12-I** show only halos as shown in **Figure 3**. These results suggest that the LC phases are N phases.

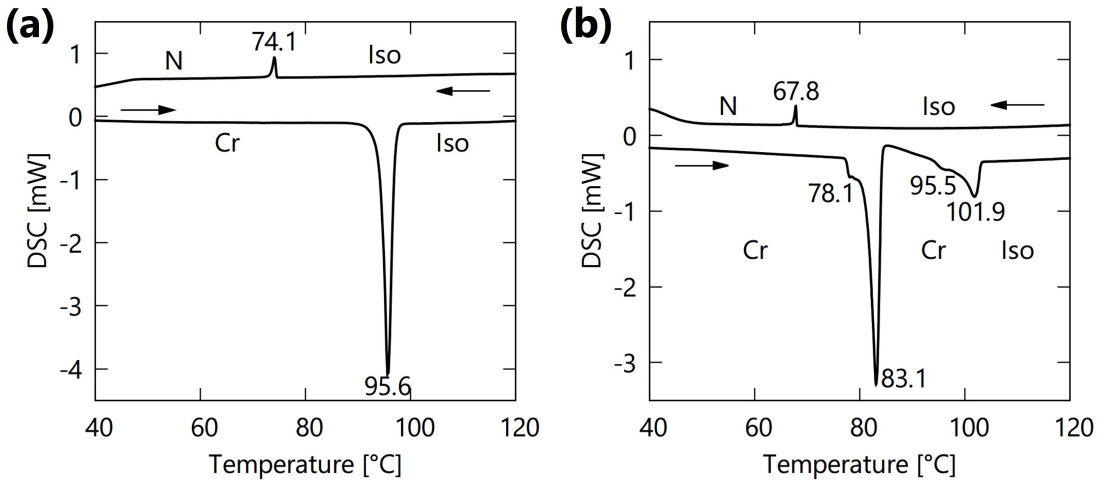

Figure 1 DSC curves of (a) (±)-**8-I** and (b) (±)-**12-I**. Transition temperatures are shown with standard notation of the phases: crystalline (Cr), nematic (N) and isotropic (Iso) phases.

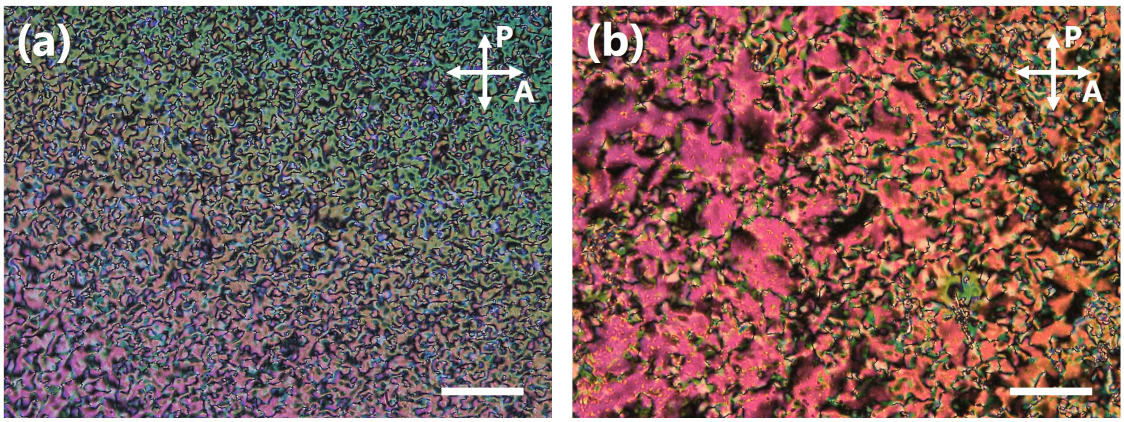

Figure 2 Polarized optical micrographs of (±)-**8-I** and (±)-**12-I** in the cooling process. (a) A

Schlieren texture for the N phase at 55 °C of (±)-**8-I**. (b) A Schlieren texture for the N phase at 55 °C of (±)-**12-I**. The orientations of polarizer (P) and analyzer (A) are shown. Scale bars correspond to 100 μm.

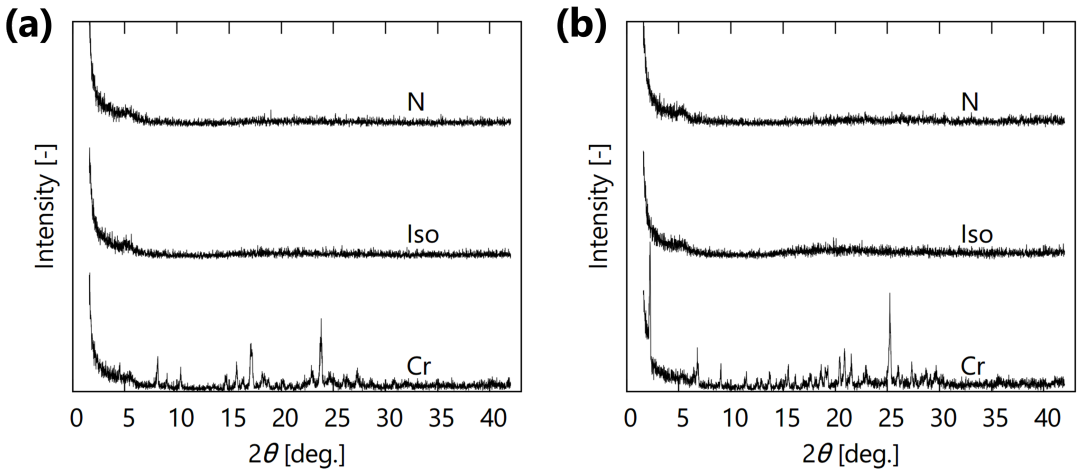

Figure 3 XRD patterns of (a) (±)-**8-I** and (b) (±)-**12-I** in Cr phase at 65 °C, Iso phase at 105 °C in the heating processes and N phase at 65 °C in the cooling processes.

Although the substituent effects of several groups and atoms on the liquid crystallinity of rod-like NR compounds have been reported, the effects of large polar groups such as the iodine atom have not been clear. In fact, a small number of iodinated LC compounds is reported, searching through one of the database of LC compounds, LiqCryst 5.2 [15]. Racemic **8-I** and (±)-**12-I** show N phase regardless of large size of the terminal iodine atom. However, iodine atom is poor substituent for NR-LC compounds compared with alkoxy chains, which are typical side groups of previously reported NR-LCs [1–3,9]. This is because that the loss of alkyl side chain and the large lateral dipole moment of NR moiety stabilize Cr phases, and then, N phases become relatively unstable. Furthermore, in many cases for LCs, long side chains tend to induce Sm phases because of interactions between alkyl chains. Actually, NR-LCs with two alkoxy chains on both sides longer than undecyloxy chain also show SmC phases [2]. However, (±)-**12-I** with dodecyloxy chain does not show any Sm phase; it is likely to be because iodine atom is too short to induce Sm phases compared to linear alkoxy chains.

3.2. Magnetic property in a lower temperature range (2-300 K)

The magnetic properties of compounds (±)-**8-I** and (±)-**12-I** are summarized in **Table 1**. The magnetic susceptibilities χ measured on a SQUID magnetometer are shown in **Figure 4a** and **4b**. The χT-T plots for both compounds obeyed the Curie-Weiss law in the temperature range between

100 and 300 K (C ~ 0.37). These results indicate that the NR moieties of (±)-**8-I** and (±)-**12-I** are chemically stable and the most NO moieties remain paramagnetic.

In the low temperature range, (±)-**8-I** shows weak antiferromagnetic intermolecular interactions (θ < 0), whereas (±)-**12-I** shows weak ferromagnetic intermolecular interactions (θ > 0). The temperature dependence of χT for (±)-**8-I** can be best fitted to a following singlet-triplet model of S = 1/2 with J/k_B = –0.691 K and α = 0.99, whereas that of (±)-**12-I** can be fitted to the same model with J/k_B = 0.734 K and α = 0.96 (**Table 1** and **Figure 4c** and **4d**),

$$\chi T = \frac{\alpha N g^2 \mu_B^2}{k_B} \frac{1}{3 + \exp(-2J/k_B T)}$$

where α denotes the radical purity of the sample, N is Avogadro constant, g is g-value, μ_B is Bohr magneton and k_B is Boltzmann constant.

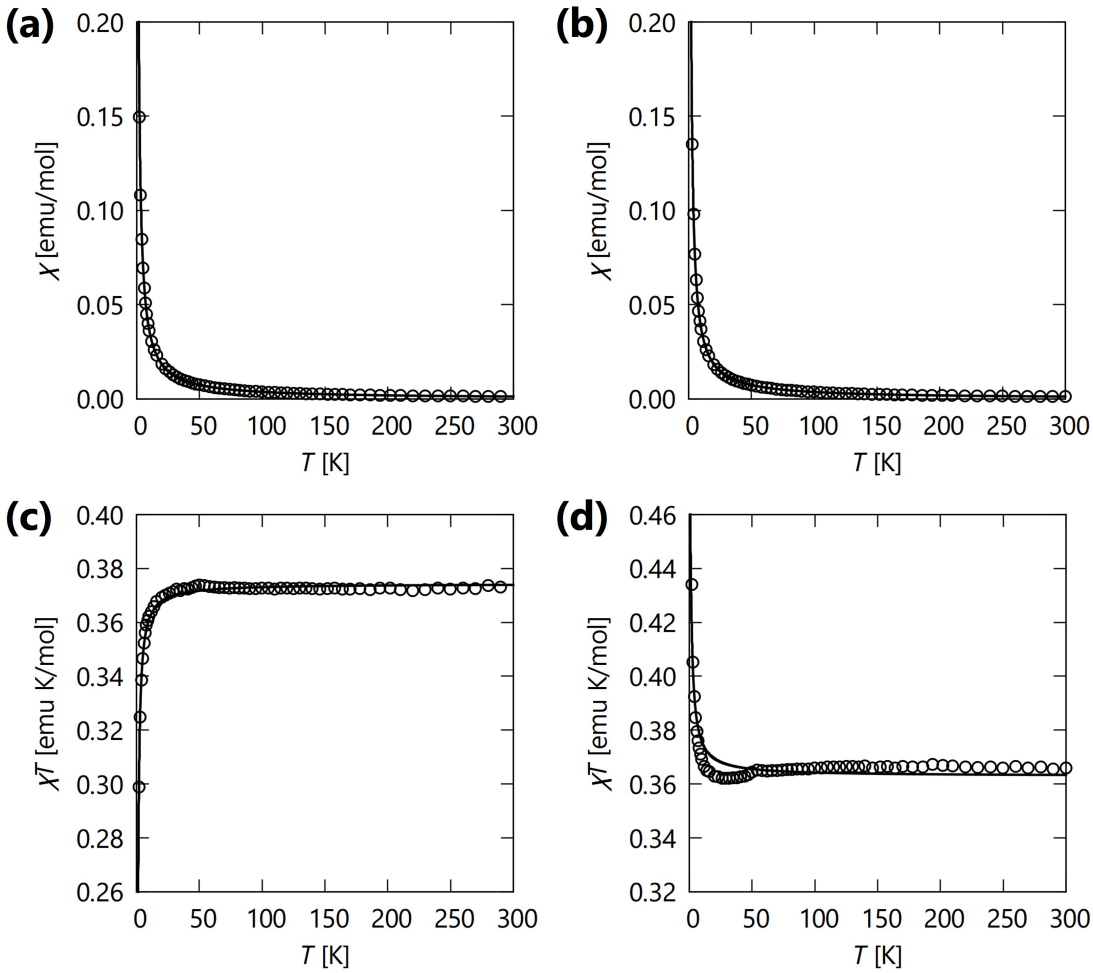

Figure 4 Temperature (T) dependence of molar magnetic susceptibility (χ) and χT-T plots of (a), (c) (±)-**8-I** and (b), (d) (±)-**12-I** at a field of 0.5 T in the heating process, respectively. Open circles represent the experimental data and solid lines show Curie-Weiss fitting curves for (a) and (b) and

theoretical singlet-triplet model fitting curves for (c) and (d).

Table 1 Magnetic properties of compounds (±)-**8-I** and (±)-**12-I**

Compound	SQUID			EPR [d]	
	C [a] [emu K mol^{-1}]	θ [b] [K]	J / k_B [c] [K]	g	a_N [mT]
(±)-**8-I**	0.373	−0.232	−0.691	2.0058	1.33
(±)-**12-I**	0.366	0.219	0.734	2.0059	1.34

[a] Curie constant. [b] Weiss temperature. [c] Obtained by curve fitting by means of singlet-triplet model. [d] Measured as THF solutions at room temperature.

To gain further insights into the observed antiferromagnetic and ferromagnetic interactions and those into the origin of the difference between exchange interactions at low temperature, we need to study the crystal structures of LC compounds (±)-**8-I** and (±)-**12-I**. Although, generally speaking, it is quite difficult to obtain single crystals of LC compounds large enough to decide the crystal structures because most of LC compounds show low-crystallinity due to their low symmetry, we could fortunately obtain a single crystal of (±)-**8-I** from hexane. The closest contact between the NO moieties (O1···O1 distance 6.625 Å) is shown in **Figure 5a**, representing that the NO group approaches a hydrogen atom of the neighboring molecule to give a 1D chain with the N1-O1···H17-C17 distance 2.611 Å. Furthermore, the intermolecular interaction between iodine atoms with I1···I1 distance 3.861 Å can also be recognized (**Figure 5b**). Perhaps, these molecular contacts and weak peaks in XRD patterns at $2\theta \sim 6$ deg. (Figure 3) indicate the terminal iodine atoms form the halogen-bonding and induce the weak ordered structure similar to Cr molecular packing.

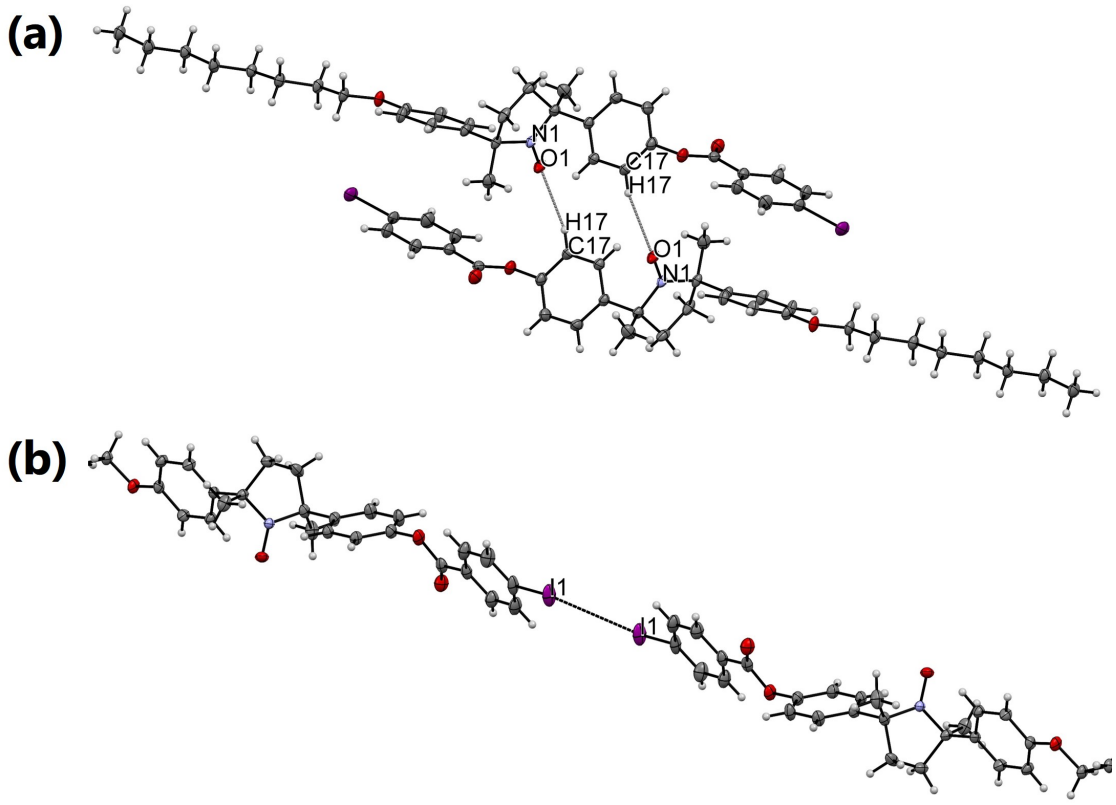

Figure 5 Crystal structure of (±)-**8-I** showing intermolecular interactions between (a) the NO radical group and the hydrogen atom, and (b) the iodine atoms.

The DFT calculations for the energy difference between the singlet and triplet states (ΔE = $E_{singlet}$ – $E_{triplet}$ = 2J for a dimer model) were performed on the dimeric coordinates of (±)-**8-I** extracted from their 1D chain structure (Figure 5a) using Gaussian 09 program package [16], giving J/k_B values of –0.458 K for UBLYP/6-311G level, which are consistent with the above experimental values[17,18]. Therefore, we can conclude that this intermolecular interaction between NO moieties in the geometry shown in **Figure 5a** is responsible to the observed antiferromagnetic property. However, the direct O1···O1 contact is may be too distant (6.625 Å) to be a source of the observed antiferromagnetic interaction. Then, we have actually computed the spin densities on N1, O1, H17, C17 atoms of a molecule in the X-ray crystal structure using Gaussian 09 program package [16] for UBLYP/6-311G level. As a result, spin density values for N1, O1 H17 and C17 atoms were obtained to be 0.441791, 0.495112, -0.000083 and 0.003405, respectively. Although the C17 atom is connected to the aminoxyl group through a lot of atoms and bonds, it has positive spin density arising from the spin polarization. Because of the negligible spin density in H17, the exchange interaction between the C17 atom and the O1 atom of the adjacent molecule (3.522 Å) renders the intermolecular exchange of spins on O1 atoms of two adjacent molecules antiferromagnetic [19].

Thus, this intermolecular spin polarization exchange coupling through C17 atom could be the origin of bulk antiferromagnetic interactions of (±)-8-I in low temperature range.

3.3. Magnetic property in high temperature range

The *g*-values and hyperfine coupling constants (a_N) were determined for THF solutions of (±)-**8-I** and (±)-**12-I** by EPR spectroscopy at a field of 0.33 T at room temperature (**Table 1**). The spectra display intense 1:1:1 triplets specific to NR compounds (**Figure 6**). To discuss the details of the temperature dependence of the magnetic properties of the condensed phases in higher temperature ranges (> 300 K), we evaluated the paramagnetic susceptibilities by variable temperature (VT) EPR spectroscopy using a quartz sample tube (**Figure 7**), which allows us to ignore the diamagnetic susceptibility (χ_{dia}) and to understand the magnetic interactions in detail [8].

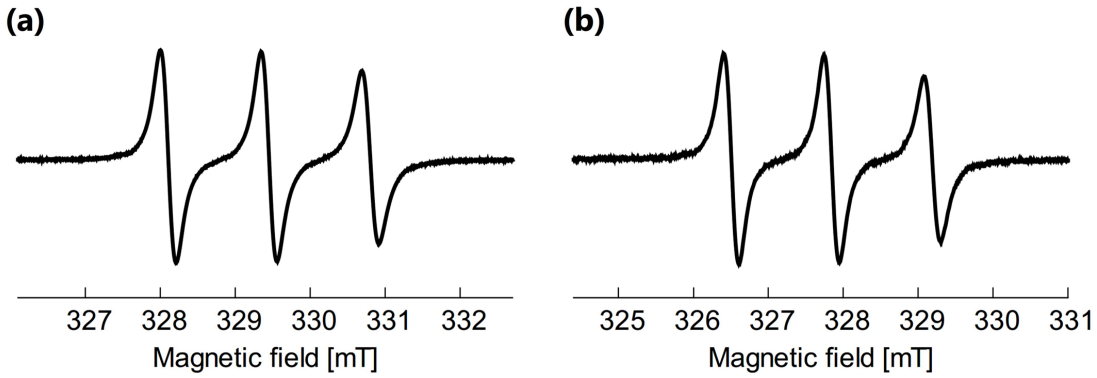

Figure 6 EPR spectra of (a) (±)-**8-I** and (b) (±)-**12-I** measured as THF solutions at room temperature.

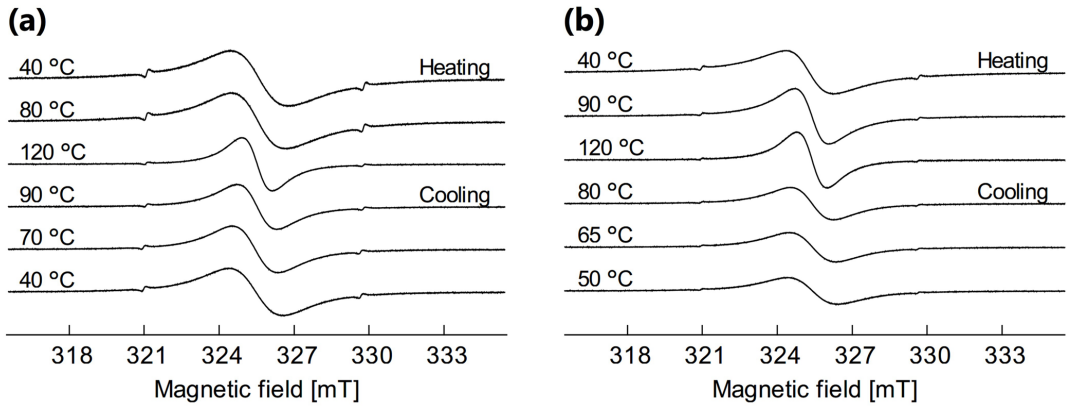

Figure 7 Selected EPR spectra of (a) (±)-**8-I** and (b) (±)-**12-I** measured at various temperatures from the crystalline phase (top) to the N phase (bottom) through the Iso phase.

Even if the EPR spectra are double-integrated, the paramagnetic susceptibility might not be accurately estimated because of the potentially presence of temperature dependent background changes. To accurately evaluate the magnetic properties from the EPR spectra without the double-integration in such a high temperature region, it is suitable to fit the experimental data with the derivative Lorentzian curve according to previously reported method [8,9],

$$I'(H) = -16I'_{\mathrm{m}}\frac{H - H_0}{\Delta H_{\mathrm{pp}}/2}\left[3 + \left(\frac{H - H_0}{\Delta H_{\mathrm{pp}}/2}\right)^2\right]^{-2}$$

where I'_{m} is the maximum peak height of the differential curve, H is the applied magnetic field, H_0 is the resonant magnetic field, and ΔH_{pp} is the peak-to-peak line width. We can easily evaluate the paramagnetic susceptibility (χ) from the parameters I'_{m}, H_0, and ΔH_{pp} by

$$\chi = \frac{2\mu_{\mathrm{B}} g I'_{\mathrm{m}} \Delta H_{\mathrm{pp}}^2}{\sqrt{3} h \nu H_1}$$

where h is Planck constant, v is the frequency of the absorbed electromagnetic wave, g is the g factor which is inversely proportional to H_0, and H_1 is the amplitude of the oscillating magnetic field. The temperature dependence of relative paramagnetic susceptibility (χ_{rel}), which is defined as

$$\chi_{\mathrm{rel}} = \frac{\chi}{\chi_0}$$

where χ_0 is the standard paramagnetic susceptibility at 40 °C in the heating run, for (±)-**8-I** and (±)-**12-I** as shown in **Figure 8**. Although the molecular structures of (±)-**8-I** and (±)-**12-I** is almost the same, the temperature dependence of χ_{rel} for (±)-**8-I** is quite different from that for (±)-**12-I** in the heating run, as shown in **Figure 8a** and **8b**. The χ_{rel} value of (±)-**8-I** slightly decreased at Cr-to-Iso phase transition (5.2% decrease compared with the Curie-Weiss fitting curve at 106 °C, $\bar{J} < 0$), whereas that of (±)-**12-I** abruptly increased at the Cr-to-Cr polymorphic transition (15.6% increase from 80 to 86 °C) and Cr-to-Iso phase transition (13.9 % increase from 102 to 106 °C, $\bar{J} > 0$); it decreases with increasing temperature in each phase, as expected from the Curie-Weiss law. In contrast to heating run, in the cooling run, χ_{rel} increases with decreasing temperature in the Iso and N phases for both samples. Similar to the case of previously reported magneto-LC effects of analogues [3,8,9], a very small change in the χ_{rel} value is commonly noted at the Iso-to-LC phase transition in the cooling run.

The abrupt changes of χ_{rel} at the phase transitions should be attributed to the molecular paramagnetic anisotropy $\Delta\chi$ and/or the changes of the intermolecular magnetic interactions J. For NR compounds, $\Delta\chi$ has been reported not to cause the changes of χ_{rel}; the contribution of $\Delta\chi$ can be expressed in terms of the change in the g value owing to magnetic-field-induced molecular reorientation, and χ_{rel} is proportional to g^2 when J is constant [8]. In fact, we examined the temperature dependence of the g value for (±)-**8-I** and (±)-**12-I** by EPR spectroscopy (**Figure 8c** and **8d**). If the changes in g-values were primarily responsible for the changes of χ_{rel} at the phase

transitions of (±)-**8-I** and (±)-**12-I**, (i) almost no χ_{rel} change would be observed at the Cr-to-Cr phase transition for (±)-**12-I** because of the very small *g* increase (0.04%) which is the largest change for the samples (**Figure 8d**), (ii) a χ_{rel} increase should occur at the Cr-to-Iso phase transition for (±)-**8-I** because of its *g*-value increase (**Figure 8a** and **8c**) and (iii) a χ_{rel} decrease should occur at the Cr-to-Cr and Cr-to-Iso phase transition for (±)-**12-I** because of its *g*-value decrease (**Figure 8b** and **8d**). However, we did not observe any of these phenomena. Accordingly, we can conclude that the $\Delta\chi$ does not contribute to the changes of χ_{rel} at the phase transitions of (±)-**8-I** and (±)-**12-I** and that the intermolecular magnetic interactions *J* would attribute to the changes of χ_{rel} value.

The intermolecular negative and positive spin-spin exchange interactions must operate the changes of χ_{rel} value for (±)-**8-I** and (±)-**12-I**, respectively. To gain an insight into the origin of the changes of χ_{rel} value, temperature dependences of ΔH_{pp} (**Figure 8e** and **8f**) were compared with that of the χ_{rel} (**Figure 8a** and **8b**). Generally, the change in ΔH_{pp} reflects the following two magnetic interactions: (a) spin-spin dipole interaction (the stronger the interactions are, the more the ΔH_{pp} increases) and (b) spin-spin exchange interaction (the stronger the interactions are, the more the ΔH_{pp} decreases). In the heating run, the decreases in ΔH_{pp} occurred in both (±)-**8-I** and (±)-**12-I**. It is resulted from the increase of spin-spin exchange interactions. In these cases, the sign of magneto-LC effects is dominated by the molecular packing manner in Cr phases possibly due to the formation of the halogen-bonding, because the magnetic interactions in the Iso and N phases similar to those in Cr phases would be statistically frequently induced by the inhomogeneous intermolecular contacts. We suppose that more strong magnetic interaction could be induced in the mobile phases by transient contacts because of molecular mobility and inhomogeneous intermolecular contacts unlike the uniform intermolecular contacts in the crystalline phases. The manner of molecular contacts in Cr phases showing antiferromagnetic ($J < 0$) and ferromagnetic ($J > 0$) interactions is likely to change in the mobile phases, and it could emphasize the increase and decrease of the magnetic susceptibilities in the Iso and N phases for (±)-**8-I** and (±)-**12-I**. Therefore, we propose that the intermolecular contacts in the fluid phases can emphasize the tendency of magnetic interactions in crystalline phases; strong intermolecular interactions appear more frequently in fluid phases than in crystalline phases.

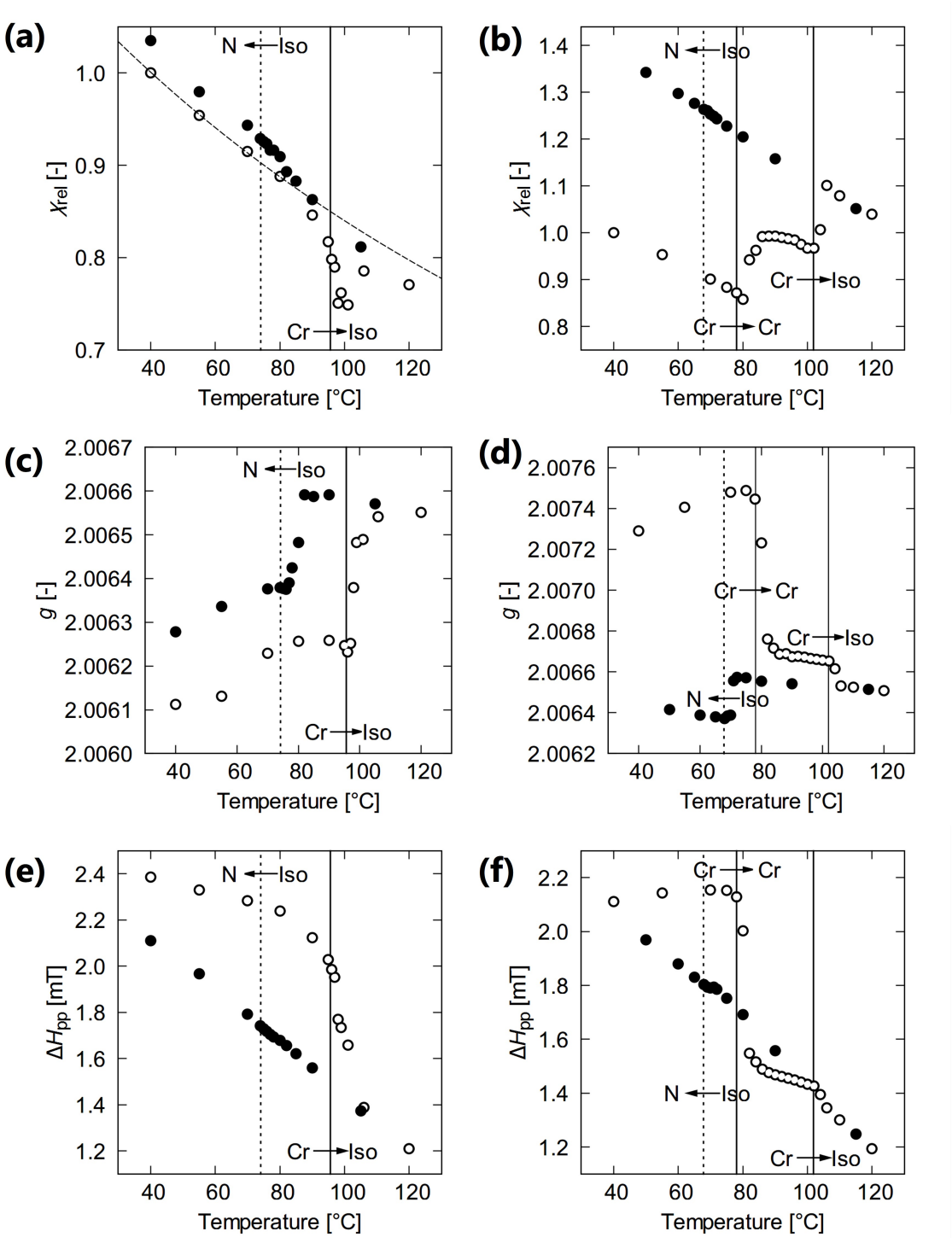

Figure 8 Temperature dependence of (a) and (b) χ_{rel}, (c) and (d) *g*-value and (e) and (f) ΔH_{pp} for (±)-**8-I** and (±)-**12-I**, respectively, which are obtained from VT-EPR spectroscopy. Open and filled circles denote the data in the heating and cooling runs, respectively. Dotted curve shows the Curie-Weiss fitting curves with temperature range of Cr phase (40–85 °C). Vertical solid and dotted lines denote the phase transition points obtained by DSC analyses in the heating and cooling runs,

respectively.

4. Conclusions

We designed and synthesized terminally iodinated NR-LCs (±)-**8-I** and (±)-**12-I** showing monotropic N phases. The iodine atom is too short and apolar as a terminal group to stabilize the LC phases of NR compounds. We found that negative magneto-LC effects ($\bar{J} < 0$) occur in the fluid phases of (±)-**8-I**, whereas positive magneto-LC effects ($\bar{J} > 0$) occur in the fluid phases of (±)-**12-I**. The experimental results indicate that the intermolecular magnetic interactions in the fluid phases are similar to those in Cr phases. We can conclude that in some cases there are only intermolecular magnetic interactions similar to those of the Cr phases in some fluid phases.

Acknowledgments

This work was supported in part by the Japan Science and Technology Agency (JST) "Precursory Research for Embryonic Science and Technology (PRESTO)" for a project of "Molecular technology and creation of new function". The authors thank Professor Rui Tamura, Kyoto University, for helpful advices and experimental supports including XRD measurement. The authors appreciate to Professor Tsuyoshi Kimura and Mr. Hiroki Ueda, Osaka University, for experimental supports including measurement of magnetic susceptibility, and to Professor Takeshi Naota and Mr. Takatoshi Maeda, Osaka University, for supports of determination of the X-ray crystal structure. The computations were performed using Research Center for Computational Science, Okazaki, Japan. T.A. is very grateful to the JSPS Research Fellowships for Young Scientists JP16J05585.

Supplementary data

CCDC 1523059 contains the supplementary crystallographic data for (±)-**8-I**. These data can be obtained free of charge via http://www.ccdc.cam.ac.uk/conts/retrieving.html, or from the Cambridge Crystallographic Data Centre, 12 Union Road, Cambridge CB2 1EZ, UK; fax: (+44) 1223-336-033; or e-mail: deposit@ccdc.cam.ac.uk.

References

[1] N. Ikuma, R. Tamura, S. Shimono, N. Kawame, O. Tamada, N. Sakai, J. Yamauchi, Y. Yamamoto, Magnetic Properties of All-Organic Liquid Crystals Containing a Chiral Five-Membered Cyclic Nitroxide Unit within the Rigid Core, Angew. Chem. Int. Ed. 43 (2004) 3677–3682. doi:10.1002/anie.200460007.

[2] N. Ikuma, R. Tamura, S. Shimono, Y. Uchida, K. Masaki, J. Yamauchi, Y. Aoki,

H. Nohira, Ferroelectric Properties of Paramagnetic, All-Organic, Chiral Nitroxyl Radical Liquid Crystals, Adv. Mater. 18 (2006) 477–480. doi:10.1002/adma.200501531.

[3] K. Suzuki, Y. Uchida, R. Tamura, S. Shimono, J. Yamauchi, Observation of positive and negative magneto-LC effects in all-organic nitroxide radical liquid crystals by EPR spectroscopy, J. Mater. Chem. 22 (2012) 6799–6806. doi:10.1039/C2JM16278D.

[4] Y. Uchida, R. Tamura, N. Ikuma, S. Shimono, J. Yamauchi, Y. Shimbo, H. Takezoe, Y. Aoki, H. Nohira, Magnetic-field-induced molecular alignment in an achiral liquid crystal spin-labeled by a nitroxyl group in the mesogen core, J. Mater. Chem. 19 (2008) 415–418. doi:10.1039/B809502G.

[5] K. Suzuki, Y. Uchida, R. Tamura, Y. Noda, N. Ikuma, S. Shimono, J. Yamauchi, Influence of applied electric fields on the positive magneto-LC effects observed in the ferroelectric liquid crystalline phase of a chiral nitroxide radical compound, Soft Matter. 9 (2013) 4687–4692. doi:10.1039/C3SM27295H.

[6] T. Akita, Y. Uchida, S. Nakagami, D. Kiyohara, N. Nishiyama, Ferronematics Based on Paramagnetic Nitroxide Radical Liquid Crystal, Crystals. 5 (2015) 206–214. doi:10.3390/cryst5020206.

[7] Y. Uchida, N. Ikuma, R. Tamura, S. Shimono, Y. Noda, J. Yamauchi, Y. Aoki, H. Nohira, Unusual intermolecular magnetic interaction observed in an all-organic radical liquid crystal, J. Mater. Chem. 18 (2008) 2950–2952. doi:10.1039/B801704B.

[8] Y. Uchida, K. Suzuki, R. Tamura, N. Ikuma, S. Shimono, Y. Noda, J. Yamauchi, Anisotropic and Inhomogeneous Magnetic Interactions Observed in All-Organic Nitroxide Radical Liquid Crystals, J. Am. Chem. Soc. 132 (2010) 9746–9752. doi:10.1021/ja101930d.

[9] Y. Uchida, K. Suzuki, R. Tamura, Magneto-LC Effects in Hydrogen-Bonded All-Organic Radical Liquid Crystal, J. Phys. Chem. B. 116 (2012) 9791–9795. doi:10.1021/jp301930k.

[10] T. Kato, J.M.J. Frechet, A new approach to mesophase stabilization through hydrogen bonding molecular interactions in binary mixtures, J. Am. Chem. Soc. 111 (1989) 8533–8534. doi:10.1021/ja00204a044.

[11] E. Barmatov, S. Grande, A. Filippov, M. Barmatova, F. Kremer, V. Shibaev, Side-chain functionalized liquid crystalline polymers and blends, 5. Order parameter for hydrogen-bonded blends of the functionalized liquid crystalline polymer with a low molecular weight dopant, Macromol. Chem. Phys. 201 (2000) 2603–2609. doi:10.1002/1521-3935(20001101)201:17<2603::AID-MACP2603>3.0.CO;2-6.

[12] A.P. Filippov, Magnetooptic properties of polymeric hydrogen-bonded liquid-crystal mixtures, J. Opt. Technol. 68 (2001) 700–703. doi:10.1364/JOT.68.000700.

[13] N. Ikuma, R. Tamura, K. Masaki, Y. Uchida, S. Shimono, J. Yamauchi, Y. Aoki,

H. Nohira, Paramagnetic FLCs Containing an Organic Radical Component, Ferroelectrics. 343 (2006) 119–125. doi:10.1080/00150190600962192.

[14] I. Dierking, Textures of Liquid Crystals, Revised edition, Wiley-VCH, Weinheim, 2003.

[15] V. Vill, LiqCryst 5.2 Database of Liquid Crystalline Compounds, Fujitsu Kyushu System Engineering (FQS), Fukuoka, 2013.

[16] M.J. Frisch, G.W. Trucks, H.B. Schlegel, G.E. Scuseria, M.A. Robb, J.R. Cheeseman, G. Scalmani, V. Barone, B. Mennucci, G.A. Petersson, H. Nakatsuji, M. Caricato, X. Li, H.P. Hratchian, A.F. Izmaylov, J. Bloino, G. Zheng, J.L. Sonnenberg, M. Hada, M. Ehara, K. Toyota, R. Fukuda, J. Hasegawa, M. Ishida, T. Nakajima, Y. Honda, O. Kitao, H. Nakai, T. Vreven, J.A. Montgomery, Jr., J.E. Peralta, F. Ogliaro, M. Bearpark, J.J. Heyd, E. Brothers, K.N. Kudin, V.N. Staroverov, R. Kobayashi, J. Normand, K. Raghavachari, A. Rendell, J.C. Burant, S.S. Iyengar, J. Tomasi, M. Cossi, N. Rega, J.M. Millam, M. Klene, J.E. Knox, J.B. Cross, V. Bakken, C. Adamo, J. Jaramillo, R. Gomperts, R.E. Stratmann, O. Yazyev, A.J. Austin, R. Cammi, C. Pomelli, J.W. Ochterski, R.L. Martin, K. Morokuma, V.G. Zakrzewski, G.A. Voth, P. Salvador, J.J. Dannenberg, S. Dapprich, A.D. Daniels, O. Farkas, J.B. Foresman, J.V. Ortiz, J. Cioslowski, D.J. Fox, Gaussian 09, Revision D.01, Gaussian, Inc., Wallingford CT, 2009.

[17] S. Yamanaka, T. Kawakami, H. Nagao, K. Yamaguchi, Effective exchange integrals for open-shell species by density functional methods, Chem. Phys. Lett. 231 (1994) 25–33. doi:10.1016/0009-2614(94)01221-0.

[18] R. Improta, K.N. Kudin, G.E. Scuseria, V. Barone, Structure and Magnetic Properties of Nitroxide Molecular Crystals by Density Functional Calculations Employing Periodic Boundary Conditions, J. Am. Chem. Soc. 124 (2002) 113–120. doi:10.1021/ja011704r.

[19] Y. Uchida, R. Tamura, N. Ikuma, K. Masaki, H. Takahashi, S. Shimono, J. Yamauchi, Antiferromagnetic interaction arising from a close contact between nitroxyl oxygen and β-methyl carbon atoms carrying an α-spin in the solid state, Mendeleev Commun. 16 (2006) 69-71. doi:10.1070/MC2006v016n02ABEH002231.